



## Vacancy Defects Induced Magnetism in Armchair Graphdiyne Nanoribbon

Somayeh Fotoohi<sup>\*1</sup>, Saeed Haji-Nasiri<sup>2</sup>

<sup>1</sup>Department of Electrical Engineering, Islamshahr Branch, Islamic Azad University, Islamshahr, Iran

<sup>2</sup>Faculty of Electrical, Biomedical and Mechatronics Engineering, Qazvin Branch, Islamic Azad University, Qazvin, Iran

(Received 22 Sep. 2019; Revised 23 Oct. 2019; Accepted 16 Nov. 2019; Published 15 Dec. 2019)

**Abstract:** Spin-polarized electronic and transport properties of Armchair Graphdiyne Nanoribbons (A-GDYNR) with single vacancy (SV), two types of configurations for double vacancy (DV1, DV2) and multi vacancy (MV) defects are studied by non-equilibrium Green's function (NEGF) combined with density functional theory (DFT). The results demonstrate that the A-GDYNR with the SV has the lowest formation energy and the most energetically favorable. The SV induces a 2.08  $\mu\text{B}$  magnetic moment while the DV2 possess no magnetism into A-GDYNR. Analyzing the band structures shows that the perturbation in A-GDYNR caused by the SV, DV1 and MV breaks the degeneracy and appears new bands around the Fermi level which indicate a strong spin splitting. Moreover, using density of states (DOS) analysis, it is illustrated that the appeared flat bands correspond to the localized states which mainly contribute by the carbon atoms near the vacancies. The calculated current-voltage characteristics for A-GDYNR with the SV, DV1, and MV reveal that the spin degeneracy is obviously broken. As well, a high spin-filtering efficiency around 90% is found at the bias voltage of 0.3V for A-GDYNR with the SV. Our findings illustrate that we can obtain A-GDYNRs with especial magnetic properties by removing carbon atoms from A-GDYNR.

**Keywords:** Armchair Graphdiyne Nanoribbons, Vacancy Defects, Non-Equilibrium Green's Function, Density Functional Theory, Formation Energy, Magnetic Moment, Spin Splitting.

### 1. INTRODUCTION

Over the past decade, many different forms of carbon allotropes such as fullerenes, carbon nanotubes, graphene, graphyne and the others have been

---

\* Corresponding author. Email: [s.fotoohi@iaau.ac.ir](mailto:s.fotoohi@iaau.ac.ir)

extensively studied due to their distinctive electronic structures and great potential for the nanoelectronic and spintronic applications [1-4]. In recent years, a new two-dimensional (2D) carbon base material, graphdiyne (GDY), has been synthesized using cross-linking reaction and annealing so it has attracted considerable attention due to its unique properties [5, 6]. Compared with graphene which has only sp<sup>2</sup>-hybridized carbon atoms, GDY is composed of sp- and sp<sup>2</sup>-hybridized carbon atoms where adjacent hexagonal rings are connected to each other by two acetylenic linkages [7]. Recent studies have reported that graphene has a zero energy band gap [8], however, GDY is a direct band gap semiconductor with a band gap value of 0.46 eV. Furthermore, the experimental measurements show that its intrinsic electron mobility is similar to that of graphene at room temperature [6,7,9]. By the standard lithographic techniques, GDY is patterned into extremely narrow ribbons, in which carriers become laterally confined in quasi-one dimensional structures known as GDY nanoribbons (GDYNRs). In terms of their edge orientation, GDYNRs are classified as either armchair- GDYNRs (A-GDYNRs) or zigzag-GDYNRs (Z-GDYNRs). Both of the A-GDYNRs and Z-GDYNRs are found to be semiconductor with direct band gaps [9,10]. Similar to graphene, GDY has attracted extensive attentions due to its electronic, transport and mechanical properties. Chemical doping has been confirmed to be an effective method to lead to various GDY derivatives with useful physical properties [11]. Recently, nitrogen-doped GDY is proposed as a desirable material for a high-powered energy storage device [12]. In the other study, sulfur doping has been used to induce robust ferromagnetic ordering into GDY and realize the coexistence of room-temperature ferromagnetism and semiconductivity in graphdiyne without extrinsic magnetic impurity [13]. Beside, in the other work, the electronic structure and magnetic properties of GDY have been tuned by the heteroatom doping [14]. Also GDYNR can be used as a molecular rectifier by modulating its electronic properties using ad-atoms [15]. Moreover, by the element doping, GDYNR can be used as a promising material for spintronic applications [16]. Theoretical studies prove that nitrogen doping leads to the formation of local magnetic moment into GDY [17]. However, the magnetic properties of GDY have not been investigated profoundly, which are very essential not only to reveal the spin polarization states in this material but also to develop GDY base spintronic devices [17-21].

Recently, it is proved that the existence of vacancies can dramatically changes the electronic and magnetic properties of graphene [19]. Similarly, it is important to study the electronic and magnetic properties of A-GDYNR in the presence of vacancies. In the practical conditions, it is hardly achievable to have a pure ideal GDYNR and real samples may naturally contain some defects. In the present work, we have investigated four types of structural vacancy defects including: (a) single vacancy (SV), (b) two types of configurations for double

vacancy (DV1 and DV2), and (c) multi vacancy (MV) defects.

## 2. COMPUTATIONAL METHODS

We perform spin-polarized DFT calculations with the SIESTA package [22]. The generalized gradient approximation (GGA) with Perdew, Burke and Ernzerhof (PBE) functional [23] is chosen for the exchange-correlation functional. SIESTA employs basis sets comprised of norm-conserving Toullier-Martins pseudopotential orbitals [24]. Each basis set is assumed numerical double- $\zeta$  plus polarization. The calculations are performed using 200 Ry cutoff energy and a density matrix convergence criteria of  $1 \times 10^{-4}$  for self-consistency. The Brillouin zone integration of the supercell is sampled with a  $1 \times 1 \times 60$  Monkhorst-Pack grid and a Gaussian smearing with a width of 0.01 eV is set in the calculations.

In order to define A-GDYNR in SIESTA package, we use the periodic boundary condition (PBC) along z-direction and the neighboring A-GDYNR in x- and y-direction should be separated by  $20 \text{ \AA}$  of vacuum space to prevent the spurious interaction between the mirror planes. The dimensions of all structures along x, y and z directions have been considered  $20 \text{ \AA}$ ,  $50.30 \text{ \AA}$  and  $39.76 \text{ \AA}$ , respectively. Furthermore, to separate a defect in a given super-cell from its nearest neighboring defects placed in the adjacent super-cells, the distance between the assumed defects is high enough (about  $d \sim 36 \text{ \AA}$ ), so the defects of the neighboring super-cells have not any interaction with each other.

In the second point of view, it is obvious that in analyzing the effect of vacancy or ad-atom, increasing the size of super-cell guaranties more real and accurate simulation results since the nature of these phenomena is random and we cannot see periodic defect in the nature. But due to the heavy and sophisticated computing, it takes too long times and needs to very powerful computers. So in the most similar studies in the current field, the authors have assumed several types vacancies or doping with the periodic boundary conditions in 2D carbon materials such as graphyne and GDY [1, 16, 20, 21, 25-28].

The edge carbon atoms are saturated by single Hydrogen atoms. All structures are fully relaxed until the maximum residual force on each atom to be less than  $0.02 \text{ eV/\AA}$ .

Electronic properties such as band structure and total density of state (TDOS) have been computed by DFT [29]. Spin-polarized transport properties, such as current-voltage characteristic and the transmission spectra have been investigated by non-equilibrium Green's function (NEGF) method [30] based on DFT in the TranSIESTA module within the SIESTA. TranSIESTA makes the ability to model open boundary conditions in the two-terminal system under different bias voltages. Each system involves a confined central scattering region where connected to two semi-infinite long electrodes. When an atomic or molecular structure is connected to the electrodes we have non-periodic system.

### 2-1. NEGF FORMALISM:

The quantum transport simulations are applied by the first-principle self-consistent non-equilibrium Green's function (NEGF) approach in combination with density functional theory.

$G_\sigma$  and  $G_\sigma^\dagger$  are the advanced and retarded Green's function matrices of the scattering region, respectively:

$$G_\sigma = [(E + i0^+)I - H - U - \Sigma_L - \Sigma_R]^{-1} \quad (1)$$

Where  $\sigma$  is  $\uparrow$  (up spin) or  $\downarrow$  (down spin) and  $H$  is the Hamiltonian matrix.  $U$  is the electrostatic potential energy achieved by solving self-consistently in three dimensions and the Poisson equation with the transport equations.  $\Sigma_L$  and  $\Sigma_R$  are the electrodes self-energy matrices which lead to the shift of the energy levels because of the interaction between the left and right electrodes respectively, and can be calculated as:

$$\Sigma_L = \tau_L^\dagger g_L \tau_L, \Sigma_R = \tau_R^\dagger g_R \tau_R \quad (2)$$

Where  $g_L$  and  $g_R$  are Green functions of the left and right electrodes surface respectively and can be effectively calculated using an iterative scheme [30].

$\tau_L$  and  $\tau_R$  are the coupling matrices between the device and the corresponding electrodes.

The carriers' spin resolved transmission probability through the device can be calculated by [30]:

$$T_\sigma(E, V_b) = \text{Trace}[\Gamma_R G_\sigma \Gamma_L G_\sigma^\dagger] \quad (3)$$

$\Gamma$  is the electrodes broadening function written as:

$$\Gamma_{L,R} = i[\Sigma_{L,R} - \Sigma_{L,R}^\dagger] \quad (4)$$

That presents the coupling at energy  $E$  between the scattering region and the left / right electrodes. The spin-dependent current that is transmitting through the central region at a given bias voltage is evaluated with the Landauer-Büttiker formula [30]:

$$I_\sigma(V_b) = \frac{e}{h} \int T_\sigma(E, V_b) [f_L(E, V_b) - f_R(E, V_b)] dE \quad (5)$$

Where  $\sigma$  is the spin component index (up/down),  $T_\sigma(E, V_b)$  is the spin-dependent transmission coefficient at the energy of  $E$  and the bias voltage of  $V_b$ .  $f_{L,R}(E, V_b)$  is the Fermi-Dirac distribution function of the left (L)/right (R) electrode.

### 3. RESULTS AND DISCUSSION

In Fig. 1, we present a pristine A-GDYNR and four types of vacancies that we have assumed in A-GDYNR. Fig. 1(a) illustrates the pristine A-GDYNR and

the labeled numbers represent the potential vacant sites. As shown in Fig. 1(a) due to the sp- and sp<sup>2</sup>-hybridized carbon networks in GDY, there are two inequivalent positions, C3 (sp carbon) or C2 (sp<sup>2</sup> carbon), that can be removed to produce SV. When we remove a single carbon atom from the sp or sp<sup>2</sup> sites, the local geometry near the vacancy site is considerably changed after the full structure optimization. However, these two structures became equivalent and we show it in Fig. 1(b).

For the DV defect, we have considered two types of configurations. Fig. 1(c,d) represent the A-GDYNRs with DV defects named as DV1 and DV2, respectively. To explore the structure of DV, we remove two neighboring carbon atoms such as C3, C4 (from sp site) or C1, C2 (from sp<sup>2</sup> site). With removing the C1 and C2 atoms in the A-GDYNR, some new bonds can be formed between C3 atom and the atoms near the vacancy so the lengths of some other bonds in the neighboring of the vacancy are changed.

To consider the MV defect in the A-GDYNR, we remove two acetylenic linkages (-C≡C-C≡C-) of one chain in the super-cell of pristine A-GDYNR. As shown in Fig. 1(e) the geometry around the vacancy site changes negligibly after the structure optimization. We clearly demonstrate that the geometric construction of A-GDYNR remains planar in all studied structures.

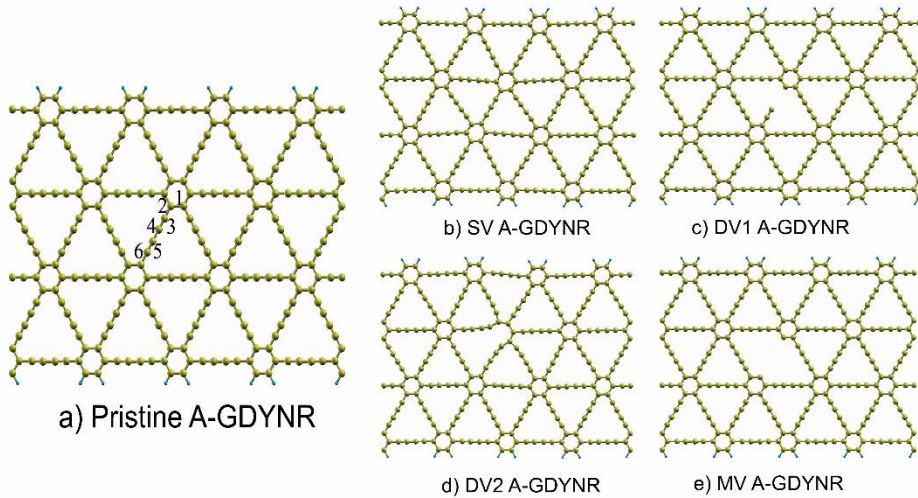


**Fig. 1** Top view of the optimized structures a) pristine A-GDYNR with the labeled numbers of vacancy sites b) SV c) DV1 d) DV1 e) MV defects.

In table 1, the formation energy ( $E_f$ ) of the A-GDYNR with defect is calculated by  $E_f = E_{vac} - E_{pristine} + N_{\mu}$ . Where,  $E_{vac}$  is the total energies of the defective A-GDYNR.  $E_{pristine}$  is the total energies of the pristine A-GDYNR. The total energies can be obtained from SIESTA package. N represents the number of

removed atoms.  $\mu$  is the chemical potential for an isolated carbon atom of bulk GDY and calculated by:

$$\mu = \frac{\text{Total energies of pristine GDY (eV)}}{\text{Number of carbon atoms in pristine GDY}} \quad (6)$$

It is important to note that the structures with larger formation energy are less stable than the structures with smaller formation energy [31].

**TABLE 1.**  
**Formation energies (eV) of A-GDYNR with different vacancies**

Vacancy Type	SV A-GDYNR	DV1 A-GDYNR	DV2 A-GDYNR	MV A-GDYNR
$E_f$ (eV)	0.71	0.95	2.04	4.17

The Formation energies of each structure are given in Table I. One finds the SV has the lowest formation energy ( $E_f = 0.71\text{eV}$ ) among the various vacancy structures. In the 1<sup>st</sup> finding, the results indicate that the SV defect is more likely to exist in A-GDYNR.

As shown in Fig. 1(d), DV2 imposes a fully reconstructed atomic structure in the surrounding of vacancies positions so this causes the formation energy of the DV2 is considerably larger than that of DV1. However, we have found no significant local geometry distortion in the A-GDYNR with DV1. This causes relatively smaller formation energy than that is in A-GDYNR with DV2.

Spin polarized calculation indicates that pristine A-GDYNR has not magnetic character. Interestingly, we find magnetic moments induced by vacancies in the A-GDYNR. The calculated magnetic moments are 2.08, 1.56, and 1.27  $\mu\text{B}$  for the A-GDYNRs with SV1, DV1, and MV respectively, whereas we find no spin polarized state in the A-GDYNRs with DV2. Consequently, in the 2<sup>nd</sup> finding the dependence of the magnetic properties on the type of the vacancy is demonstrated.

In Fig. 2 we illustrate spatial iso-surface of the spin polarization charge density of the A-GDYNR when the vacancies are included. The red and blue iso-surfaces represent the up and down spin densities at 0.002 e/bohr<sup>3</sup>, respectively. The A-GDYNR with DV2 is not shown in this figure, since it is found to be non-magnetic, as already discussed. The corresponding spin polarized charge densities, shown in Figs. 2(a-c), indicate that the induced magnetic moments are mainly localized around the vacancy sites. Clearly, the SV has a larger effect on the spin polarization of the A-GDYNR and this is compatible with the results that are reported in Table 2.

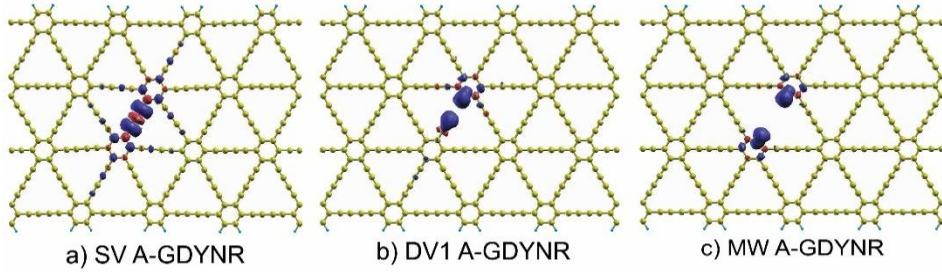


**Fig 2.** The spin density difference (up spin - down spin) of magnetic structures. The A-GDYNR with (a) SV, (b) DV1, and (c) MV defects. The red and blue colors are corresponding to the up and down spins. The iso-surface is taken to be  $0.002 \text{ e}\text{\AA}^{-3}$ .

Fermi Energy for the pristine and A-GDYNRs with the assumed defects are given in Table 2.

The comparisons reveal that in all of the assumed structures the Fermi level is shifted to the valance band of the A-GDYNR. In the 3<sup>rd</sup> finding, this result suggests that vacancy defects can be used as an effective way to produce p-type doping in the A-GDYNRs.

**TABLE 2.**

The values of magnetic moment, Fermi energy and the energy band gap ( $E_g$ ) for the assumed structures.

Structure Type	Perfect A-GDYNR	SV A-GDYNR	DV1 A-GDYNR	DV2 A-GDYNR	MV A-GDYNR
Magnetic Moment ( $\mu\text{B}$ )	0	2.08	1.56	0	1.27
Fermi Energy (eV)	-6.35	-6.45	-6.66	-6.44	-6.69
$E_g$ (eV)	0.82	0.42	0	0.42	0.82

Fig. 3 represents the spin polarized band structures and density of states (DOSs) of the A-GDYNR with the assumed defects. In addition, the band structure and density of state for the pristine A-GDYNR are given in Fig. 3(a). It is obvious that the pristine A-GDYNR is semiconductor with a direct band gap of 0.82 eV at the  $\Gamma$ -point. This result is in good agreement with previously reported results [9,11].

In particular, the pristine A-GDYNR indicates symmetric up and down spin bands, which offers that it is a nonmagnetic semiconductor. Fig. 3(b) shows the spin polarized band structure and density of states (DOS) of the A-GDYNR with SV. The result illustrates that the SV induces the defect states in the middle of the band gaps. However, both of the up and down spin bands display

semiconducting behavior with 0.75 and 0.55 eV band gap, respectively, which are smaller than that of the pristine A-GDYNR (0.82 eV). The result shows that the up spin flat band is occupied and the down spin flat band is unoccupied in the vicinity of the Fermi level. These two flat bands correspond to the localized states at the Carbon atoms around the vacancy site that will be shown in Fig. 4(a). From another point of view, in the plotted DOSs in Fig. 3(b), it is seen that the up and down spin DOSs are highly asymmetric, reveal that the A-GDYNR with SV is magnetic.

The band structures and DOSs of A-GDYNR with DV1 and DV2 are presented in Figs. 3(c,d). In the A-GDYNRs with DV, the band structures show a structural dependency on the configuration of the vacancies. Figure 3(c) shows the spin polarized band structure and density of state for DV1. It is notable that the down spin band structure behaves as a half-metal due to a state crossing the Fermi level that is completely localized near the vacancies as will be shown in Fig. 4(b). Moreover, the up spin shows semiconducting behavior with a direct band gap of 0.83 eV. The down density of state for the A-GDYNR with DV1 illustrates a peak at the Fermi level that is related to the electrons trapped in the localized states near the vacancy defect (Fig. 2(b)).

In contrast, as shown in Fig. 3(d), we find semiconducting behavior for both of the up and down spins in the A-GDYNR with DV2. Also, as can be seen in this figure, the A-GDYNR with DV2 shows symmetric up and down spin bands, which in the 4<sup>th</sup> finding, offers that the A-GDYNR with DV2 is a nonmagnetic semiconductor.

Fig. 3(e) gives the spin polarized band structure and DOS of the A-GDYNR with MV. Interestingly, both of the up and down spin bands show semiconducting behaviors. The up and down spin band gaps are 0.75 and 0.55 eV, respectively, which are smaller than that of the pristine A-GDYNR (0.82 eV). As shown in this figure, the band structure is substantially modified which is found a spin splitting due to the vacancy. In the 5<sup>th</sup> finding, it is worth noting that the spin polarization is sensitive to the type of the vacancies.

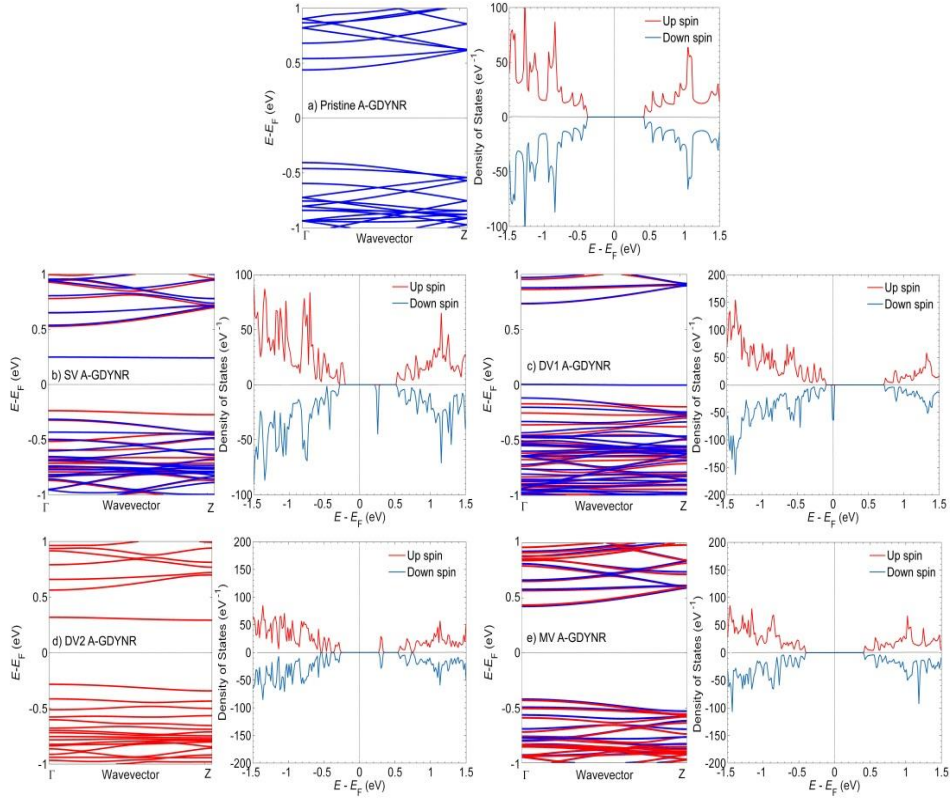
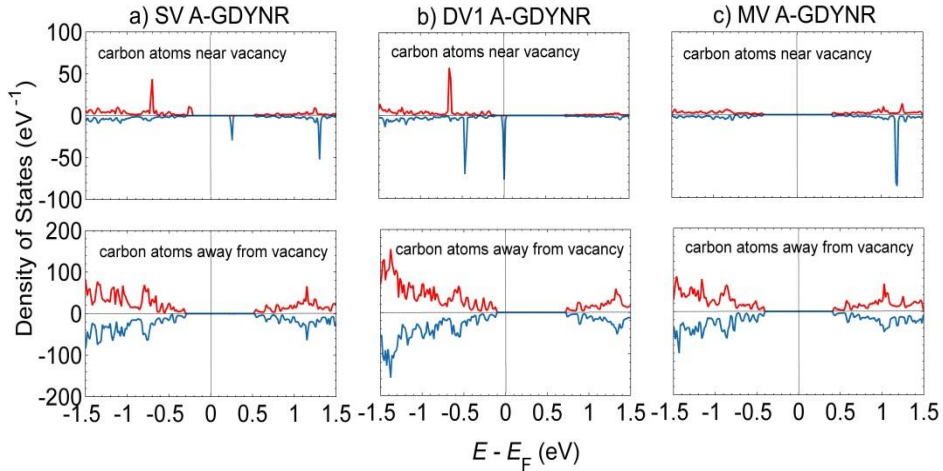


Fig 3. The spin-polarized band structures and density of states for (a) pristine (b) SV (c) DV1 (d) DV2 (e) MV A-GDYNR. The band structures of up spin (down spin) electrons are illustrated by red (blue) lines. The Fermi level is indicated by dashed black lines.

To clarify more on this issue that the flat states are localized on some carbon atoms around the vacancies sites, we divide the super-cell into two components: (1) the carbon atoms near the vacancies and (2) the carbon atoms away from the vacancies. Then, we calculate the DOS contribution of each component. Fig. 4 shows that the spin states of the carbon atoms near the vacancy split degeneracy. It leads to the spin-polarized states and resulting in asymmetry of the up and down spin states. For each of the assumed defects, the comparison reveals that the large peaks are related to the localized states which mostly contributed by the carbon atoms around the vacancies.

Moreover, the Carbon atoms away from the vacancies represent almost identical DOSs. It confirms that they play no role in the magnetic properties.



**Fig. 4.** Density of States (DOSs) curves for the A-GDYNRs with a) SV, (b) DV1 and (c) MV: the upper panels are for DOSs of carbon atoms near the vacancies and the lower panels are for DOSs of the carbon atoms away from the vacancies. The up spin and down spin states are denoted by the positive and negative values, respectively. The Fermi level is set to be zero.

In the next stage, we calculate the  $I-V_b$  characteristics of the open two-probe structures when they are biased. In doing so, we consider the A-GDYNRs super-cells as shown in Figs. 1(a-e) that are connected to two semi-infinite pristine A-GDYNRs, on the left and right electrodes. The currents for the up and down spins of the defective A-GDYNRs as well as the pristine one are given versus the applied bias voltage ( $V_b$ ) in Figs. 5-1(a-d) and Figs. 5-2(a-d) by the linear and logarithm scales respectively. Clearly, the  $I-V_b$  characteristic of the pristine A-GDYNR has semiconductor behavior that is in good agreement with its band structure and density of state, in which the threshold voltage is about 0.82V. This result is in good accordance with the other reports [9,11].

As shown in this figure, obvious current appears when the bias voltage is larger than the bandgap. More interestingly, in the 6<sup>th</sup> finding, the negative differential resistance (NDR) phenomenon can be observed at the bias voltage of  $V_b = 1.9$  V. As shown in Fig. 5-1(a), for the A-GDYNR with SV, the current of the up spin state grows rapidly from 0.8 to 1.8 V and then decreases. So, a NDR characteristic appears. However, it is different for the down spin state in which the current increases along with increasing the bias voltages. Moreover, it can be seen that the currents are spin polarized.

As illustrated in Fig. 5-1(b), for the A-GDYNR with DV1, both of the up and down spin currents increase with an increase in the voltage bias. Moreover, according to the result, the down spin current is larger than the up spin current for the similar bias voltage. The spin degeneracy in the A-GDYNR with DV1 is

obviously broken and the current becomes strongly spin dependent. However, as shown in Fig. 5-1(c) in the A-GDYNR with DV2 A-GDYNR the up and down spin currents through the structure, are degenerated completely.

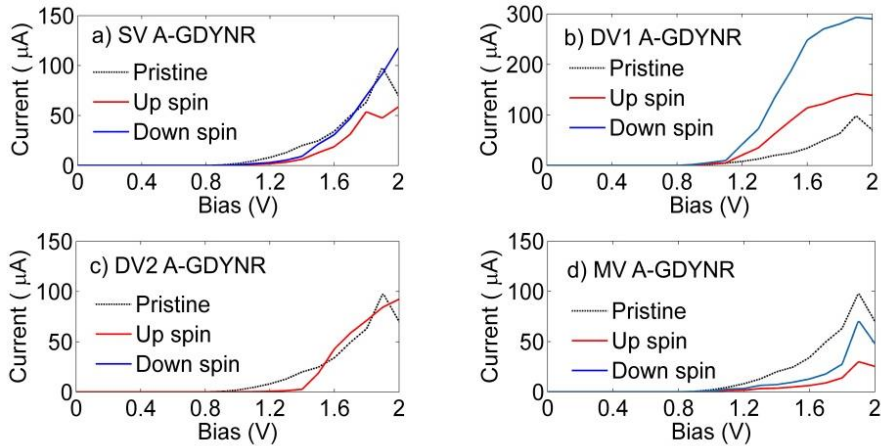
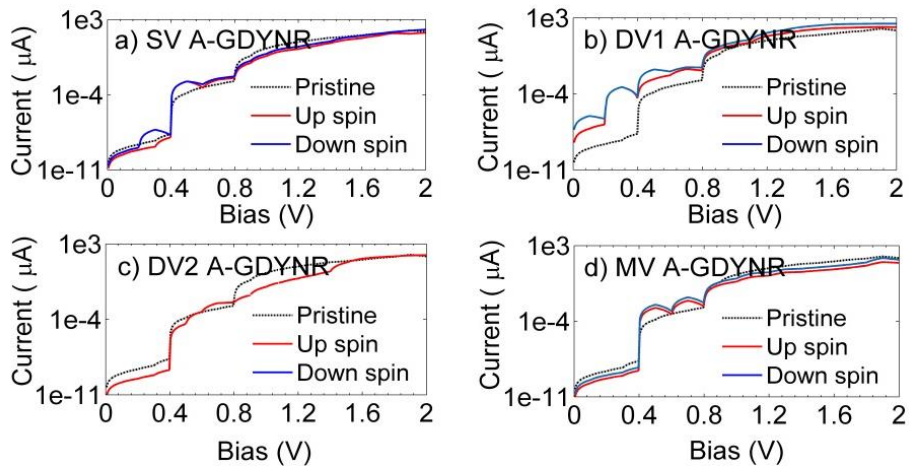


Fig. 5-1. The linear scale spin-polarized current for the A-GDYNR with (a) SV, (b) DV1 (c) DV2 and (d) MV under the bias voltages.



**Fig. 5-2.** The logarithm scale spin-polarized current for the A-GDYNR with (a) SV, (b) DV1 (c) DV2 and (d) MV under the bias voltages.

**Fig. 5.** The spin-polarized current-voltage characteristic for the A-GDYNR with a) SV, (b) DV1 (c) DV2 and (d) MV in comparison with that of a similar super-cell for the pristine A-GDYNR (dashed lines) (currents are in linear scale in Fig. 5-1. and are in logarithm scale in Fig. 5-2.). The up and down spin electrons are presented by solid red and blue lines, respectively.

As shown in Fig. 5-1(d), for the A-GDYNR with MV, the down spin current is obviously larger than the up spin current and the spin NDR is obviously appeared for both of the up and down spin currents. So, in the 7<sup>th</sup> finding, it presents a spin-polarized characteristic for using in the spin filtering devices. Moreover, the NDR behavior is observed in the similar bias to that is in the pristine A-GDYNR. We observe that the current of A-GDYNR with DV1 is obviously larger than that of the other structures. This is due to the high density of states below the Fermi level (Fig. 3(c)) that are related to the extra transport channels. Therefore, the electrons can be transmitted easily from the energy bands in left electrode to the energy bands in the right electrode through the scattering region.

According to the results, the down spin currents are larger than the up spin currents for the similar bias voltage in the A-GDYNRs with SV, DV1 and MV. This result is in good agreement with the relative spin polarization charge density shown in Fig. 2.

To better estimate the current under the low-biased conditions, we illustrate the logarithm scale of the current versus the linear scale voltage bias in Fig. 5-2. As shown in this figure, the A-GDYNRs with SV, DV1, and MV have spin-polarized currents in the low bias conditions.

To confirm the spin-polarized current–voltage characteristics of the two-probe structures, we have shown the transmission spectra for both spin channels at different bias voltages in Figs. 6 and 7.

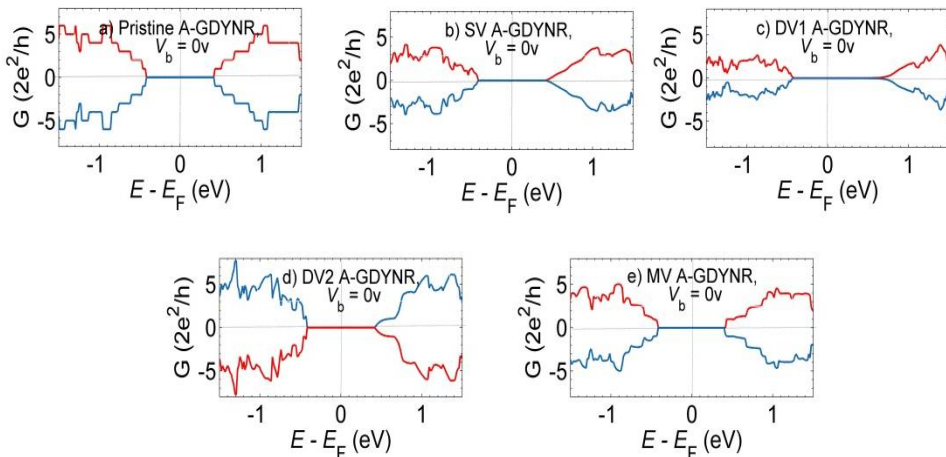


**Fig. 6.** The spin-polarized transmission spectra at the bias of 0 V for (a) Pristine (b)SV, (c) DV1 (d) DV2 and (e) MV structures. The red lines present the up spin channel and the blue lines present the down spin channel.

As shown in Fig. 6, the zero transmission is corresponding to the energy window of  $-0.41 \text{ eV} \leq E - E_F \leq 0.41 \text{ eV}$ . This is due to the fact that in all of the two probe structures, the electrodes are pristine A-GDYNRs with a  $0.82 \text{ eV}$  band gap value.

Moreover in order to have a comprehensive comparison, transmission spectra for both of the spin channels at the bias voltages of  $0.3, 0.5, 0.7, 1.5, 1.7$  and  $2.0 \text{ V}$  are shown in Figs. 7-1 to Fig. 7-6, respectively.

As is known, the spin-polarized current through the structures is calculated by integrating the transmission function over the bias window using the Landauer-Büttiker formalism [30]. Hence, the value of the current depends on the transmission coefficients in the bias window (between the two vertical dotted lines).

From Figs. 7-1 to 7-3, it can be seen that up to the bias voltage of  $V_b = 0.8 \text{ V}$ , the transmissions coefficients are too small and almost are near the zero in the bias windows, which leads to a very weak spin current in the bias voltages of  $0.3, 0.5$  and  $0.7 \text{ V}$ .

However, from Figs. 7-4 to 7-6 it can be seen that as the bias voltage increases above  $0.8 \text{ V}$  for all of the assumed structures, the nonzero transmission coefficients appear in the bias windows that provide new channels for the electron transport and the spin current are significantly enhanced. Typically, in Figs. 7-4(c) to 7-6(c) for A-GDYNR with DV1, it can be easily seen that in the bias window there exists high down spin transmission coefficients which make contributions to the down spin current, so it is larger. Also we observe that the current of the A-GDYNR with DV1 is obviously larger than that of the other structures. These are consistent with the  $I-V_b$  diagrams of Figs. 5(a-d)

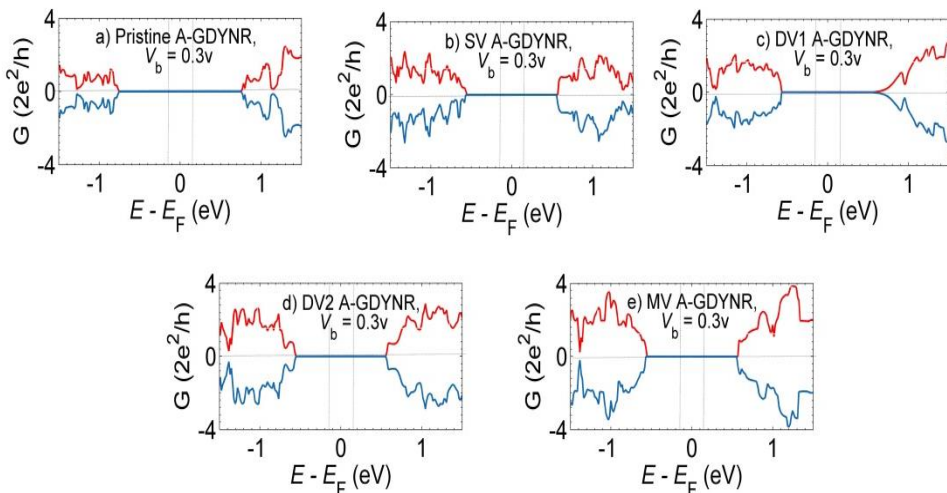


**Fig. 7-1.** The spin-polarized transmission spectra at the bias of  $0.3 \text{ V}$

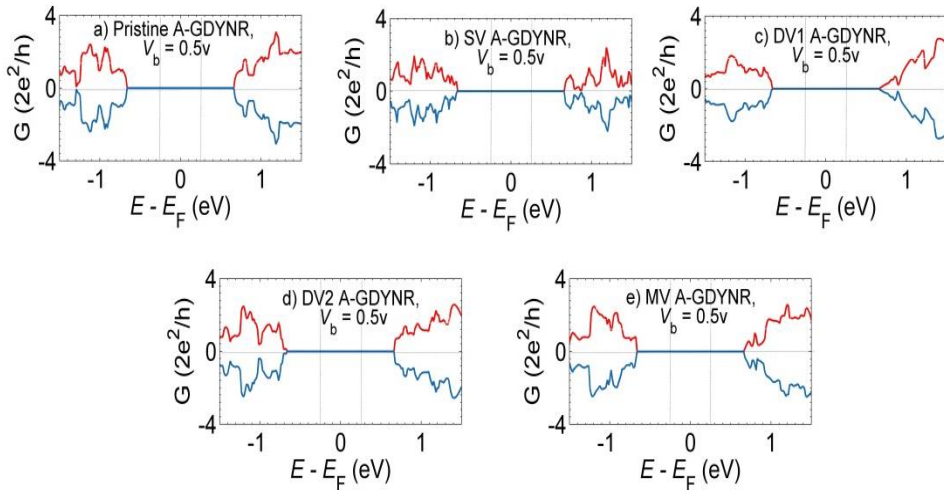


**Fig. 7-2.** The spin-polarized transmission spectra at the bias of 0.5 V

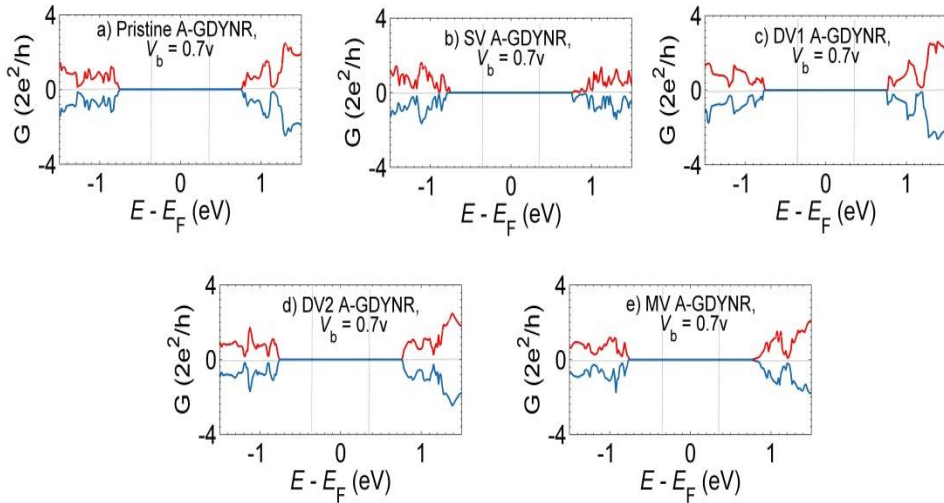


**Fig. 7-3.** The spin-polarized transmission spectra at the bias of 0.7 V

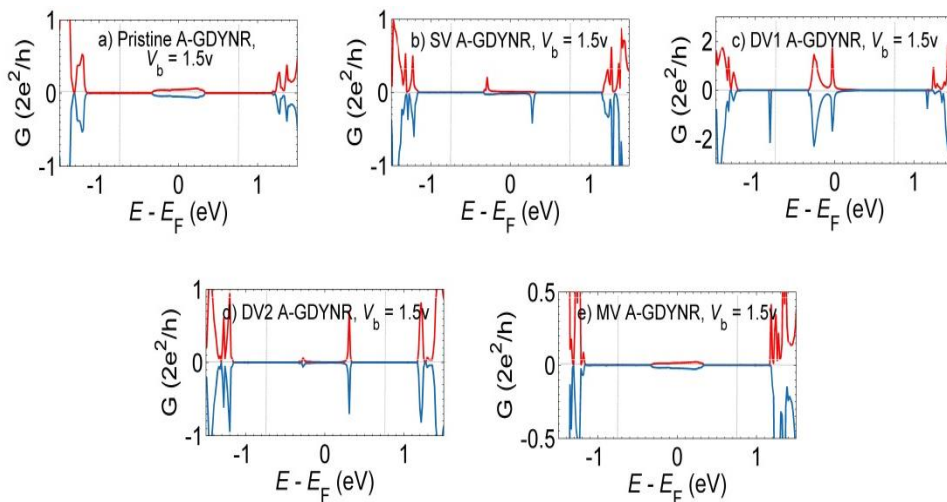


**Fig. 7-4.** The spin-polarized transmission spectra at the bias of 1.5 V

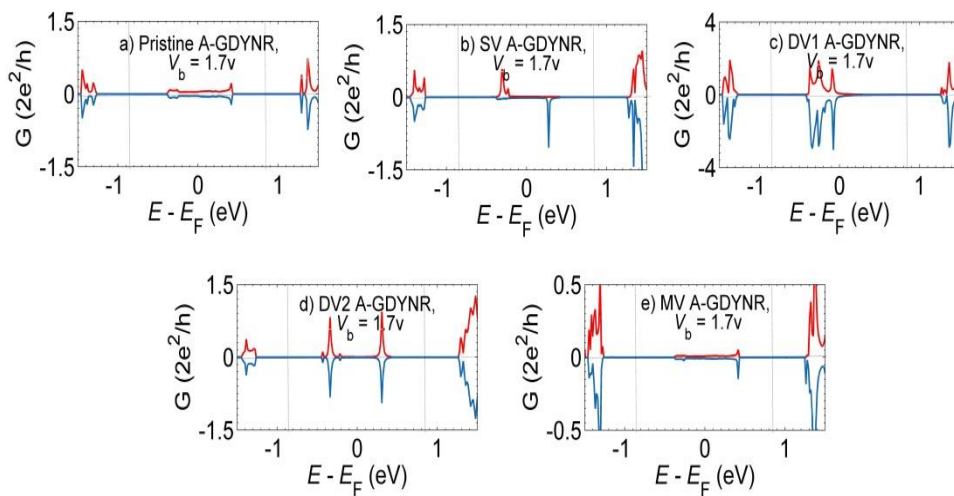


**Fig. 7-5.** The spin-polarized transmission spectra at the bias of 1.7 V

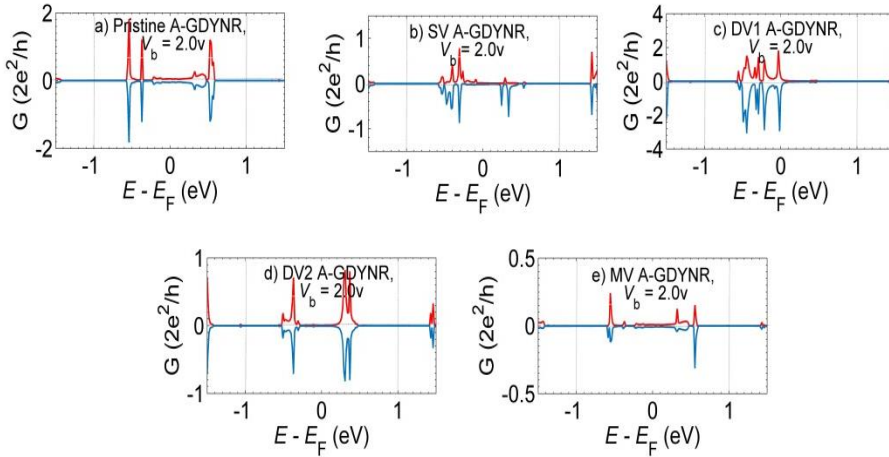


**Fig. 7-6.** The spin-polarized transmission spectra at the bias of 2.0 V

**Fig. 7** The spin-polarized transmission spectra at the bias of 0.3 V (Fig. 7-1) to 2.0 V (Fig. 7-6) for (a) Pristine (b) SV, (c) DV1 (d) DV2 and (e) MV structures. The red lines present the up spin channel and the blue lines present the down spin channel. The region between the two vertical dotted lines is the bias window.

Finally, we compute spin filtering efficiency (SFE) defined as  $SFE = |I_{up} - I_{down}| / |I_{up} + I_{down}|$ , where  $I_{up}$  and  $I_{down}$  represent the up and down spin currents, respectively at the bias region [32] (Fig. 8(a-c)). It is clearly seen that the SFEs of the structures are strongly depending on the bias voltages and have non-linear behaviors. The maximum SFEs are 90%, 85% and 40% for the A-GDYNRs with SV, DV1 and MV at the bias voltage of 0.3V, 0.1V and 0.9V, respectively. Furthermore, for the A-GDYNRs with SV and DV1, the maximum SFE appears under the low bias voltages. However, maximum SFE of the A-GDYNR with MV occurs under the high bias voltage.

Consequently, in the 8<sup>th</sup> finding, it is revealed that the spin filtering effect is dependent to the bias voltage and the type of vacancy defect. It is noteworthy to say, it is the first time that the SFE for the defected A-GDYNR is calculated. The proposed structures may bring the promise potential for the applications of the defected A-GDYNRs in nano-scale spintronic devices.

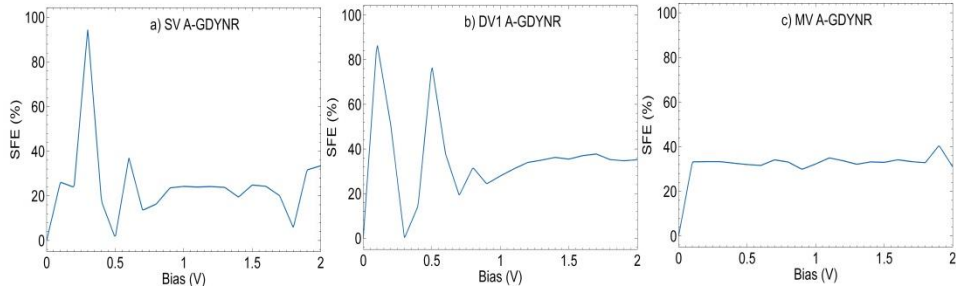


**Fig. 8.** SFE as a function of bias voltage for the A-GDYNR with a) SV, b) DV1 and c) MV

Finally, in order to have comparison with the other similar researches in this area we have summarized these works in table 3. The structures, types of the defects and the final result of them are included in this table. As it shown, each type of defect has its impact on the assumed structure. This can lead to the structural rearrangement, some changes in the magnetic moment and the type of semiconductor with changing the  $E_g$  value.

**TABLE 3.**

**A brief comparison by the other similar defects in Graphite and Graphyne**

Reference	Structure	Kind of defect	The Result
[33] Ugeda et. al. Title: Missing Atom as a Source of Carbon Magnetism	Graphite With single-atom vacancy	removing C atom from $\alpha$ , $\beta$ site	Removing a C atom from an $\alpha$ site generates a stronger magnetic moment
[34] Kang et. al. Title: Single-atom vacancy induced changes in electronic and magnetic properties of graphyne	$\alpha$ , $\beta$ , $\gamma$ graphyne (Gy) sheet with single-atom vacancy	removing C1 (sp carbon) or C2 (sp <sup>2</sup> carbon) is denoted v1 and v2, respectively.	1- The position of the removed C atom plays an important role in tuning the electronic structure of graphyne and showed different influences based on the type of graphyne. 2- A single-atom vacancy can lead to an in-plane structural rearrangement. 3-Removing C1 makes $\alpha$ Gy a p-type semiconductor, while removing C2 results in an n-type semiconductor. 4-For $\beta$ Gy, v1- $\beta$ Gy is a p-type semiconductor, while v2- $\beta$ Gy exhibits metallic character. 5- $\gamma$ Gy is half-metallic regardless of whether C1 or C2 is removed.

			<p>6- Magnetic moments were obtained 1.21, 1.14, 1.34, 1.11, 1.85, and 1.74 <math>\mu\text{B}</math> for <math>v1-\alpha\text{Gy}</math>, <math>v2-\alpha\text{Gy}</math>, <math>v1-\beta\text{Gy}</math>, <math>v2-\beta\text{Gy}</math>, <math>v1-\gamma\text{Gy}</math>, and <math>v2-\gamma\text{Gy}</math>, respectively.</p> <p>7- The single-atom vacancy can induce stronger magnetization in <math>\gamma\text{Gy}</math> than in the other two models.</p>
<p>[35] Wu et. al. Title: Effects of Double-atom Vacancy on the Electronic Properties of Graphyne: A DFT Investigation</p>	<p><math>\alpha</math>, <math>\beta</math>, <math>\gamma</math> graphyne (Gy) sheet with double-atom vacancy (DAV)</p>	<p>There are several ways to insert DAV into <math>\alpha</math>, <math>\beta</math>, <math>\gamma</math> Gy due to their hybrid network of <math>sp^2</math> (DAV1, DAV2 in <math>\alpha\text{Gy}</math>) (DAV1, DAV2, DAV3 in <math>\beta\text{Gy}</math>) (DAV1, DAV2, DAV3 in <math>\gamma</math> Gy)</p>	<p>1- DAV led to in-plane structural rearrangement for all three of the Gy systems.</p> <p>2- The position of DAV is a crucial factor in the manipulation of the electronic properties of <math>\alpha\text{Gy}</math> and <math>\beta\text{Gy}</math> as compared with <math>\gamma\text{Gy}</math>.</p> <p>3- DAV1-<math>\alpha\text{Gy}</math> is a metallic ferromagnetism with a magnetic moment of 1.99 <math>\mu\text{B}</math>, while DAV2-<math>\alpha\text{Gy}</math> is a semiconductor with an <math>E_g</math> of 0.17 eV.</p> <p>4- DAV1-<math>\beta\text{Gy}</math> is an antiferromagnetic semiconductor, and DAV2-<math>\beta\text{Gy}</math> and DAV3-<math>\beta\text{Gy}</math> show metallic characteristics.</p> <p>5- All of the defective systems for <math>\gamma\text{Gy}</math> are nonmagnetic semiconductors, and the position of the vacancy can slightly change the <math>E_g</math> value.</p>

#### 4. CONCLUSION

Spin-dependent electronic transport properties of vacancy defects in A-GDYNR have been investigated by means of NEGF method in combination with DFT. We have assumed four types of defects in A-GDYNR that are named as SV, DV1, DV2 and MV. It is demonstrated that the geometric structure of A-GDYNR remains planar in all of the four considered defects. The results reveal the SV defect is energetically more stable than the other types of vacancy defects in A-GDYNR. In addition, it is illustrated introducing vacancy defect is an effective way to produce p-type doping in A-GDYNR due to the Fermi level shift to the valance band.

Calculations of the electronic structures reveal that vacancies have a significant effect on electronic properties of A-GDYNR where DV1 shows half-metallic band structure but in contrary, the other vacancies display semiconducting band structures. Moreover, A-GDYNRs with SV, DV1, and MV display magnetic properties due to the strong spin splitting property of the energy levels. For A-

GDYNR with SV, the defect induce states which are highly splitted and appeared in the band gap, leads to have the largest magnetic moment in comparison with the other types of the assumed defects. Spin polarization charge densities show that the carbon atoms far from the vacancy defects do not have obvious spin polarization, and magnetic moments are mainly localized in the carbon atoms near the vacancies. Furthermore, the result of spin polarized charge densities shows that SV has larger impact on the spin polarization of A-GDYNR. The SV can induce a 2.08  $\mu\text{B}$  magnetic moment into A-GDYNR, while this value equals zero in A-GDYNR with DV2. Consequently, the dependence of the magnetic properties on the configuration of the vacancies is demonstrated. Spin-polarized transport properties for A-GDYNRs with SV, DV1 and MV are found since the spin degeneracy of current is completely broken and the down spin current becomes larger than the up spin current for the same bias voltages. We have observed that the current of A-GDYNR with DV1 is obviously larger than that of the other structures. This is due to the high density of states below the Fermi level that are related to the extra transport channels. Besides, the A-GDYNR with SV induces large spin-filtering effect where it is around 90% at the bias voltage of 0.3 V. The major novelty of this work is that the findings may bring great promise for applications of the defected A-GDYNRs in nano-scale spintronic devices.

## REFERENCES

- [1] M. Ghorbanzadeh Ahangari, *Effect of defect and temperature on the mechanical and electronic properties of graphdiyne: A theoretical study*, Physica E 66, (2017, Feb.), 140-147.  
Available:  
<https://www.sciencedirect.com/science/article/pii/S1386947714003592>
- [2] H. Rahimi, *Absorption Spectra of a Graphene Embedded One Dimensional Fibonacci Aperiodic Structure*, Journal of Optoelectrical Nanostructures 3(4), (2018, autumn), 45-58.  
Available:  
[http://jopn.miau.ac.ir/article\\_3259\\_fd0b0ef6f20c392b449ca69ad1d2f918.pdf](http://jopn.miau.ac.ir/article_3259_fd0b0ef6f20c392b449ca69ad1d2f918.pdf)
- [3] A. Abdikian, G. Solookinejad, Z. Safi, *Electrostatics Modes in Monolayered Graphene*, Journal of Optoelectrical Nanostructures 1(2), (2016, summer), 1-8.  
Available:[http://jopn.miau.ac.ir/article\\_2044\\_8b18c60167baa91a0369f64730d82f40.pdf](http://jopn.miau.ac.ir/article_2044_8b18c60167baa91a0369f64730d82f40.pdf)

- [4] H. Faezinia, M. Zavvari, *Quantum modeling of light absorption in graphene based photo-transistors*, Journal of Optoelectrical Nanostructures 2(1), (2017, winter), 9-20.  
Available: [http://jopn.miau.ac.ir/article\\_2196\\_127072bb11b75037590ab77092f278c6.pdf](http://jopn.miau.ac.ir/article_2196_127072bb11b75037590ab77092f278c6.pdf)
- [5] G. Li, Y. Li, H. Liu, Y. Guo, Y. Lia and D. Zhua, *Architecture of graphdiyne nanoscale films*, Chemical Communication 46(19), (2010), 3256-3258.  
Available: <https://pubs.rsc.org/en/content/articlelanding/2010/cc/b922733d#!divAbstract>
- [6] L. Lin, H. Pan, Y. Chen, X. Song, J. Xu, H. Liu, Sh. Tang, Y. Du, N. Tang, *Identifying the stacking style, intrinsic bandgap and magnetism of pristine graphdiyne*, Carbon 143, (2019, Mar.), 8-13.  
Available:  
<https://www.sciencedirect.com/science/article/pii/S0008622318309126>
- [7] Y. Zheng, Y. Chen, L. Lin, Y. Sun, H. Liu, Y. Li, Y. Du and N. Tang, *Intrinsic magnetism of graphdiyne*, Applied Physics Letters 111(3), (2017, Jul.), 033101-5.  
Available:  
<https://aip.scitation.org/doi/abs/10.1063/1.4993916?journalCode=apl>
- [8] S. Fotoohi, M. K. Moravvej-Farshi, R. Faez, *Electronic and transport properties of monolayer graphene defected by one and two carbon ad-dimers*, Applied Physics A 116(4), (2014, Sep.), 2057-2063.  
Available: <https://link.springer.com/article/10.1007/s00339-014-8400-9>
- [9] M. Long, L. Tang, D. Wang, Y. Li, Zh. Shuai, *Electronic Structure and Carrier Mobility in Graphdiyne Sheet and Nanoribbons: Theoretical Predictions*, ACS-Nano 5(4), (2011, Mar.), 2593-2600.  
Available: <https://pubs.acs.org/doi/10.1021/nn102472s>
- [10] X. Chen, D. Fang, Y. Zhang, B. Gong and Sh. Zhang, *Novel electronic transport of zigzag graphdiyne nanoribbons induced by edge states*, EPL (Europhysics Letters) 107(5), (2014, Aug.), 1-6.  
Available: <https://iopscience.iop.org/article/10.1209/0295-5075/107/57002>
- [11] Ch. Ge, J. Chen, Sh. Tang, Y. Du, and N. Tang, *Review of the Electronic, Optical, and Magnetic Properties of Graphdiyne: From Theories to Experiments*, ACS Applied Material Interfaces 11(3), (2019, Jan.), 2707-2716.  
Available: <https://www.ncbi.nlm.nih.gov/pubmed/29701448>

- [12] Sh. Zhang, H. Du, J. He, Ch. Huang, H. Liu, G. Cui and Y. Li, *Nitrogen-Doped Graphdiyne Applied for Lithium-Ion Storage*, ACS Applied Materials & Interface 8(13), (2016, Apr.), 8467-8473.  
Available: <https://www.ncbi.nlm.nih.gov/pubmed/26998614>
- [13] M. Zhang, H. Sun, X. Wang, H. Du, J. He, Y. Long, Y. Zhang, Ch. Huang, *Room-Temperature Ferromagnetism in Sulfur-Doped Graphdiyne Semiconductors*, Journal of Physical Chemistry 123(8), (2019), 5010-5016.  
Available: <https://pubs.acs.org/doi/10.1021/acs.jpcc.8b10507>
- [14] Zh. Feng, Y. Ma, Y. Li, R. Li, J. Liu, H. Li, Y. Tang, X. Dai, *Importance of heteroatom doping site in tuning the electronic structure and magnetic properties of graphdiyne*, Physica E 114, (2019, Oct.), 1-9.  
Available:  
<https://www.sciencedirect.com/science/article/pii/S1386947719305831>
- [15] Zh. Zhe, L. Qun, W. Xuanmin Zhu, *Modulating the electronic properties of graphdiyne nanoribbons*, Carbon 66, (2014, Jan.), 504-510.  
Available:  
<https://www.sciencedirect.com/science/article/pii/S0008622313008804>
- [16] X. Chen, P. Gao, L. Guo, Y. Wen, Y. Zhang, Sh. Zhang, *Two-dimensional ferromagnetism and spin filtering in Cr and Mn-doped graphdiyne*, Journal of Physics and Chemistry of Solids 105, (2017, Jun.), 61-65.  
Available:  
<https://www.sciencedirect.com/science/article/abs/pii/S0022369716312495>
- [17] M. Zhang, X. Wang, H. Sun, N. Wang, Q. Lv, W. Cui, Y. Long and Ch. Huang, *Enhanced paramagnetism of mesoscopic graphdiyne by doping with nitrogen*, Scientific Reports 7, (2017), 1-10.  
Available: <https://www.nature.com/articles/s41598-017-11698-9>
- [18] B. Bhattacharya, N. Bedamani Singh and Utpal Sarkar, *Tuning the magnetic property of vacancy-defected graphyne by transition metal absorption*, AIP Conference Proceedings 1665, (2015), 0500661-3.  
Available: <https://aip.scitation.org/doi/10.1063/1.4917707>
- [19] M. Valencia, M. J. Caldas, *Vacancy in graphene: insight on magnetic properties from theoretical modeling*, Physical Review B 96, (2017, Apr.), 1254311-9.  
Available: <https://arxiv.org/abs/1704.01906>
- [20] B. Kang, H. Ai, J. Yong Lee, *Single-Atom Vacancy Induced Changes in Electronic and Magnetic Properties of Graphyne*, Carbon 116, (May, 2017), 113-119.

Available:

<https://www.sciencedirect.com/science/article/pii/S0008622317300787>

- [21] S. Fotoohi, S. Haji-Nasiri, *Spin-dependent electronic transport properties of transition metal atoms doped  $\alpha$ -armchair graphyne nanoribbons*, Physica E 98, (2018, Apr.), 159-167.

Available:

<https://www.sciencedirect.com/science/article/pii/S1386947717311980>

- [22] J. M. Soler, E. Artacho, J. D. Gale, A. Garcia, J. Junquera, P. Ordejon, D. Sanchez-Portal, *The SIESTA method for ab initio order-N materials simulation*, Journal of Physics: Condensed Matter 14(11), (2002, Mar.), 2745-2779.

Available:

<https://iopscience.iop.org/article/10.1088/0953-8984/14/11/302/meta>

- [23] J. P. Perdew, K. Burke and M. Ernzerhof, *Generalized Gradient Approximation Made Simple*, Physical Review Letters 77(18), (1996, Oct.), 3865-3868.

Available: <https://www.ncbi.nlm.nih.gov/pubmed/10062328>

- [24] N. Troullier and J. Martins, *A straightforward method for generating soft transferable pseudopotentials*, Solid State Communication 74, (1990, May), 613-616.

Available:

<https://www.sciencedirect.com/science/article/pii/0038109890906866>

- [25] S. Kim, Jin Yong Lee, *Doping and vacancy effects of graphyne on SO<sub>2</sub> adsorption*, Journal of Colloid and Interface Science 493, (2017, May), 123-129.

Available: <https://www.ncbi.nlm.nih.gov/pubmed/28088564>

- [26] J. Yun, Y. Zhang, M. Xu, K. Wang, Zh. Zhang, *Effect of single vacancy on the structural, electronic structure and magnetic properties of monolayer graphyne by first-principles*, Materials Chemistry and Physics 182, (2016, Jul.), 439-444.

Available: [https://www.researchgate.net/publication/305630814\\_Effect\\_of\\_single\\_vacancy\\_on\\_the\\_structural\\_electronic\\_structure\\_and\\_magnetic\\_properties\\_of\\_monolayer\\_graphyne\\_by\\_first-principles](https://www.researchgate.net/publication/305630814_Effect_of_single_vacancy_on_the_structural_electronic_structure_and_magnetic_properties_of_monolayer_graphyne_by_first-principles)

- [27] S. GolafroozShahri, M. R. Roknabadi, R. Radfar, *Spin-dependent structural, electronic and transport properties of armchair graphyne nanoribbons doped with single transition-metal atom, using DFT calculations*, Journal of Magnetism and Magnetic Materials 443, (2017, Dec.), 96-103.

Available:

<https://www.sciencedirect.com/science/article/abs/pii/S0304885317308028>

- [28] B. Kang, H. Shi, F Wang, J Yong Lee, *Importance of doping site of B, N, and O in tuning electronic structure of graphynes*, Carbon 105, (2016, Apr.), 156-162.

Available:[https://www.researchgate.net/publication/301319525\\_Importance\\_of\\_doping\\_site\\_of\\_B\\_N\\_and\\_O\\_in\\_tuning\\_electronic\\_structure\\_of\\_graphynes](https://www.researchgate.net/publication/301319525_Importance_of_doping_site_of_B_N_and_O_in_tuning_electronic_structure_of_graphynes)

- [29] C. Fiolhais, F. Nogueira, M. Marques, *A Primer in Density Functional Theory*, 1st ed., Springer, Heidelberg, 2003, 100-138.

Available: <https://link.springer.com/book/10.1007/3-540-37072-2>

- [30] S. Datta, *Quantum Transport: Atom to Transistor*, 2nd ed., Cambridge, Cambridge University Press, 2005, 183-216.

Available:<https://www.amazon.com/Quantum-Transport-Transistor-Supriyo-Datta/dp/0521631459>

- [31] L. Li, S. Reich, and J. Robertson, *Defect energies of graphite: Density-functional calculations*, Physical Review B 72, (2005, Nov.), 1841091-10.

Available:

<https://journals.aps.org/prb/abstract/10.1103/PhysRevB.72.184109>

- [32] Sh. Abdulkader Tawfik, X. Y. Cui, S. P. Ringer and C. Stampfl, *Large spin-filtering effect in Ti-doped defective zigzag graphene nanoribbon*, Physical Chemistry Chemical Physics 18(24), (2016), 16224-16228.

Available:<https://pubs.rsc.org/en/content/articlelanding/2016/cp/c6cp01601d#!divAbstract>

- [33] M. M. Ugeda, I. Brihuega, F. Guinea, and J. M. Gomez-Rodriguez, *Missing Atom as a Source of Carbon Magnetism*, Physical Review Letters 104, (2010, Mar.), 0968041- 0968044.

Available:

<https://journals.aps.org/prl/abstract/10.1103/PhysRevLett.104.096804>

- [34] B. Kang, H. Ai , J. Yong Lee, *Single-atom vacancy induced changes in electronic and magnetic properties of graphyne*, Carbon 116, (2017, May), 113-119.

Available:

<https://www.sciencedirect.com/science/article/pii/S0008622317300787>

- [35] S. Wu, Y. Yuan, H. Ai, J. Yong Lee, and B. Kang, *Effects of Double-atom Vacancy on the Electronic Properties of Graphyne: A DFT Investigation*, Physical chemistry chemical physics 35, (2018), 1-6.

Available: <https://pubs.rsc.org/en/content/articlelanding/2018/cp/c8cp03359e#!divAbstract>